



Analytical model for LLC resonant converters in operation below resonance

Daniel Neuner · Michael Hartmann

Received: 7 October 2022 / Accepted: 29 November 2022 / Published online: 17 January 2023
 © The Author(s) 2023

Abstract Electric cars are a great opportunity for reducing greenhouse gas emissions caused by transportation. High-power chargers are required to charge electric vehicles in a reasonable amount of time and considerably increase the driving range. As these high-power chargers currently need to be isolated with respect to the grid, the LLC converter topology emerged as a very good solution for implementing the required isolated DC/DC converter stage. The analysis and optimal design of this resonant converter stage are a challenging task, as some models are oversimplified, resulting in major errors and a high amount of processing time. This paper presents a novel analytical model for the LLC converter operating below resonance, which allows accurate modeling of the converter with minimal effort. In most cases, no iterations are required, and a comparison to numerical results taken from time domain simulations shows that the relative deviation of the proposed model stays far below 1% for a wide range of operating conditions.

Keywords Resonant converter · LLC · Operation below resonance · Analytical model · Electric vehicle charger

Analytisches Modell zur Beschreibung von LLC-Resonanzwandlern im unterresonanten Betrieb

Zusammenfassung Das durch Elektrofahrzeuge gegebene Potenzial zur Verringerung verkehrs- und transportbedingter Treibhausgasemissionen ist immens. Um die Langstreckenfähigkeit derartiger Verkehrsmittel

zu verbessern, werden Hochleistungsladegeräte benötigt. Letztere müssen gegenüber dem Netz isoliert sein. Eine Wandler-Topologie, mit der es möglich ist, das zu realisieren, und die sich nicht zuletzt aufgrund ihrer hohen Effizienz als vielversprechend herauskristallisiert hat, ist der LLC-Resonanzwandler. Die Analyse sowie das optimale Design dieses Resonanzwandlers sind oft aufwändig und herausfordernd, da die beschreibenden Modelle häufig zu stark vereinfacht sind. Dies führt wiederum zu großen Abweichungen und erfordert einen mehrstufigen Optimierungsprozess, was zu erheblichem Zeitaufwand im Designprozess führen kann.

Diese Arbeit stellt einen neuartigen analytischen Modellansatz zur Beschreibung des LLC-Wandlers im unterresonanten Betrieb vor. Dies erlaubt eine Modellierung des Wandlers mit minimalem Aufwand. In einem weiten Betriebsbereich ist das Modell in der Lage, eine rein analytische Lösung ohne numerische Iterationen zu liefern. Ein Vergleich der Ergebnisse mit Zeitbereichssimulationen zeigt, dass die relative Abweichung des vorgeschlagenen Modells für einen breiten Bereich von Betriebspunkten weit unter 1% liegt.

Schlüsselwörter Resonanter Wandler · LLC · Unterresonanter Betrieb · Analytisches Modell · Ladegerät Elektrofahrzeug

1 Introduction

In recent years, high power chargers for electric vehicles emerged and have become more and more important. Therefore, applicable converter structures have been subject of research [2, 14, 18]. Beside the price pressure, also the technical requirements for the converter are demanding due to the high power level. Striving for smaller size and less weight, the resulting power density and the thermal stress of the

D. Neuner and M. Hartmann are OVE members.

D. Neuner (✉) · M. Hartmann
 Electric Drives and Machines Institute, Graz University of
 Technology, Inffeldgasse 18/I, 8010 Graz, Austria
neuner@tugraz.at

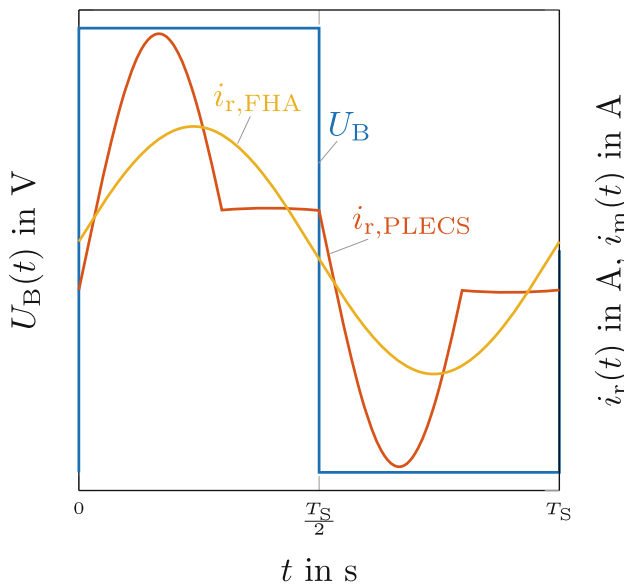


Fig. 1 Qualitative waveforms of the bridge voltage U_B and the resonant current obtained from PLECS simulation software ($i_{r,PLECS}$) as well as from using the FHA method ($i_{r,FHA}$)

components is tremendous [8], [3]. This can only be handled by proper component selection and efficient converter design. Among other topologies, the LLC resonant converter [12] as shown in Fig. 2, emerged to be an ideal solution, as it provides humongous advantages for the intended use, especially in operation below resonance (OBR).

In order to find the optimal parameter set, an accurate model for converter design is required. A very well known approach is the so called First Harmonic Approximation (FHA), where the resonant current is approximated by using solely the fundamental wave. More details of this simplified approach can be found in [1, 5, 17].

Nonetheless, this model shows some severe drawbacks as it is not usable for conduction loss calculation nor for direct converter design due to its inaccuracy, which is also addressed in [7]. To underpin that, Fig. 1 qualitatively shows a simulated resonant current waveform using PLECS simulation software and the corresponding waveform obtained with the FHA method in OBR operation mode.

However, it can still be used to investigate specific converter details, e.g. to analyze the zero voltage switching behavior [13].

Other approaches trying to address the drawbacks of FHA, e.g. taking also higher harmonics into account, numerical approximations [6] or modified gain models [11] reach far better results but are still an approximation, or rely on numerical models.

For converter cell optimization, an analytical model is essential. Beside several time domain analysis approaches for optimal design, e.g. [9], [16], this paper presents a novel analytical approach, where only a very small number of iterations is necessary in order

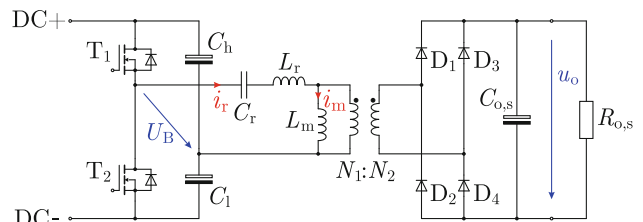


Fig. 2 Basic structure of the LLC resonant converter

to describe the time dependent converter quantities in steady state condition. Hence the calculations require minimum effort. The solution presented in this paper is restricted to the OBR, but can also be extended to other operation modes, i.e. operation above resonance (OAR). Also the load range has to be restricted to obtain the certain operation behavior mapped in this approach, but could be easily extended with the models derived in this work.

In Sect. 2, the basic converter structure with its possible operation modes is discussed briefly. In Sect. 3, the new analytical model for operation in OBR is derived. The model results for different operating points are compared to PLECS-Simulations and presented in Sect. 4. A conclusion is finally given in Sect. 5.

2 Basic Converter Structure

The basic structure of the LLC resonant converter is given in Fig. 2. The input stage is implemented using a half bridge and the other leg of the transformer primary winding is connected to two capacitors C_h and C_l respectively. Alternatively, also a full bridge can be used. The duty cycle is set to 50% and the converter output voltage can be controlled by changing the switching frequency.

The resonant tank is given through the resonant capacitance C_r , a resonant inductance L_r and the magnetizing inductance L_m of the transformer. Depending on the operating condition and the converter design, the resonant inductance L_r is (partly) implemented by the stray inductance of the transformer. Those quantities are decisive for the converter behavior and must therefore be chosen properly. Characteristic for operating the converter is the higher ratio between resonant and magnetizing inductance $\frac{L_r}{L_m}$. The ratio is addressed by constructive transformer design measures, where an airgap is inserted into the transformer [15]. This leads to a sufficiently high increase of the magnetizing current, providing the ability of zero voltage switching of the bridge leg semiconductors also in OBR operating mode, which subsequently contributes to an increase of total efficiency.

Isolation of the topology is achieved by the transformer with turns ratio $\frac{N_1}{N_2}$.

The output stage on the secondary site of the transformer is built by a full bridge rectifier. The output ca-

capacitance is assumed to be sufficiently high in order to provide satisfactory ripple free output voltage.

Finally, the load is modelled by a resistance.

The fundamental operating modes can be classified as follows:

- Resonant Operation (RO)
- Operation Above Resonance (OAR)
- Operation Below Resonance (OBR)

Of course those operating modes can be further subdivided considering other characteristic behaviors as discussed in [10]. However, this is not needed in this work.

Due to the structure of the LLC converter, one design dominating resonance frequency arises which is given by

$$f_r = \frac{1}{2\pi\sqrt{L_r \cdot C_r}} \quad (1)$$

For RO, the switching frequency of the converter is equal to the resonance frequency. This operation mode represents the boundary between OBR and OAR. Accordingly, for OAR the switching frequency is above the resonance frequency. The big advantage of this operating mode is that zero voltage switching is given for any operating point [4].

Finally, the switching frequency is smaller than the resonance frequency for OBR. Zero voltage switching is also achievable in this operating mode, but depends on the load condition as well as on the switching frequency [15]. If the operating point is designed properly, ZVS is achieved with the additional side effect of a softer turn-off of the rectifier diodes [15], contributing further to the total efficiency.

For the named reasons, operating mode OBR is selected in this work as it leads to minimal losses.

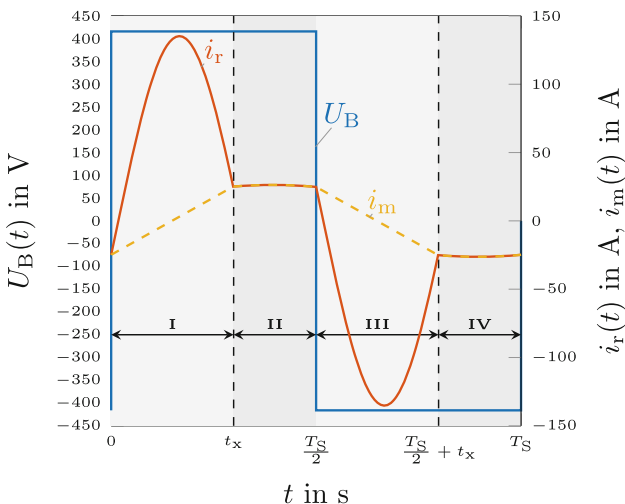


Fig. 3 Bridge voltage U_B , resonant current i_r and magnetizing current i_m of the LLC resonant converter in OBR mode for $U = 416\text{V}$, $f_s = 3\text{kHz}$, $C_r = 10\ \mu\text{F}$, $L_r = 0.1\ \text{mH}$, $L_m = 1\ \text{mH}$, $C_o = 3\ \text{mF}$, $R_o = 10\ \Omega$, $\frac{N_1}{N_2} = 1$

In Fig. 2, the Bridge Voltage U_B with amplitude U , the resonant current i_r , as well as the magnetizing current i_m are depicted. Fig. 3 shows the corresponding voltage and current waveforms for a certain operating point in OBR. In a wide frequency range, this is the characteristic behavior. One can see that the steady state is characterized through half wave symmetry, which is valid for all quantities. On one hand it implies that the converter can be fully described by only knowing one half wave, on the other hand it can be used to formulate helpful integral conditions which will be discussed in the next chapter.

3 Analytical Model

In the following, a novel analytical model of the LLC resonant converter in OBR mode is derived. Having a closer look to the converter structure, it appears that the transformer has to be considered accordingly. This is achieved by taking the transformer turns ratio into account, subsequently transforming the load represented through $R_{o,s}$ as well as the output capacitor $C_{o,s}$ to the primary side. In the following, R_o and C_o are considered to be the primary sided resistance and capacitance. Furthermore, four energy storage elements appear. Setting up a differential equation in time domain would therefore lead to a system with 4th order, where also initial conditions need to be considered. Thus, it is way more convenient to switch to the Laplace domain.

By subdividing the cycle into intervals strategically in order to get rid of the non linearity caused by the full bridge rectifier (a potential nonlinear behavior of other circuit elements, e.g. due to magnetic saturation is neglected), each interval shows an individual characteristic which can be described through a linear electrical network. Applying the Laplace Transform therefore is straight forward.

Accordingly, as shown in Fig. 3, the switching cycle is subdivided into four intervals given through I, II, III and IV respectively:

- **Interval I** = $\{0 \leq t \leq t_x\}$
For $t \in \text{I}$, the resonant current differs from the magnetizing current. Hence, power is transmitted from the input to the output. The corresponding diodes are conducting during this period and the bridge rectifier can be neglected in this case. The corresponding equivalent model including the initial conditions is shown in Fig. 4.
- **Interval II** = $\{t_x \leq t \leq \frac{T_s}{2}\}$
During $t \in \text{II}$, the magnetizing current i_m is equal to the resonant current i_r . According to Kirchhoff's Current Law, the current through the transformer is zero. Thus, the equivalent model decouples into two parts given through the secondary output part and the primary resonant input part. The corresponding equivalent model with the initial conditions considered is given in Fig. 5.

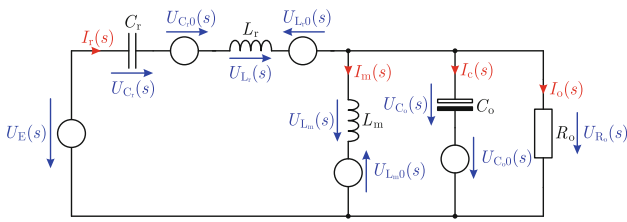


Fig. 4 Equivalent model for the interval $t \in \text{I}$

- Interval III** = $\{\frac{T_S}{2} \leq t \leq \frac{T_S}{2} + t_x\}$
 The case $t \in \text{III}$ is similar to $t \in \text{I}$. However, the bridge voltage changes sign compared to Interval I. Therefore, the voltage arrow at the input has to be inverted accordingly. Fig. 6 shows the resulting equivalent circuit with the initial conditions included.
- Interval IV** = $\{\frac{T_S}{2} + t_x \leq t \leq T_S\}$
 The equivalent model with the initial conditions valid for interval $t \in \text{IV}$ represented in Fig. 7 is similar to $t \in \text{II}$. Identical to interval III, the voltage arrow is inverted according to the apparent input voltage.

For the equivalent models given in Fig. 4 to Fig. 7, the input voltage $U_E(s)$ is stated generally. As it is intended here to operate the input bridge with duty cycle $\delta = 0.5$, a symmetrical square wave signal with cycle time T_S is obtained. Thus

$$U_B = \begin{cases} +U & \text{for } 0 \leq t < \frac{T_S}{2} \\ -U & \text{for } \frac{T_S}{2} \leq t < T_S \end{cases} \quad (2)$$

is valid here.

Subsequently, regarding to the intervals given in Fig. 3, with $\mathcal{L}\{1\} = \frac{1}{s}$ in mind the following can be stated for all four time intervals

$$U_E(s) = \frac{U}{s}. \quad (3)$$

Please remind that the voltage polarity has been inverted for the intervals III and IV (see also Figs. 6 and 7).

3.1 Derivation of the model for interval I and III

For the model given in Fig. 4, Kirchhoff's law provides:

$$I_r(s) = I_m(s) + I_c(s) + I_o(s) \quad (4)$$

$$\frac{U}{s} = U_{C_r}(s) + U_{C_r}(s) + U_{L_r}(s) - U_{L_r}(s) + U_{L_m}(s) - U_{L_m}(s) \quad (5)$$

$$U_{L_m}(s) = U_{C_o}(s) + U_{C_o}(s) + U_{L_m}(s) \quad (6)$$

$$U_{R_o}(s) = U_{C_o}(s) + U_{C_o}(s) \quad (7)$$

Please remind that for interval III, U has to be replaced by $-U$, and $U_{C_o}(s)$ by $-U_{C_o}(s)$ due to the inverted polarity (see also Figs. 4 and 6). Eqs. (4) to (7) can be rewritten to

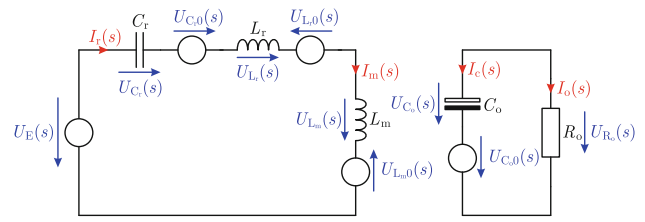


Fig. 5 Equivalent model for the interval $t \in \text{II}$

$$\begin{bmatrix} 0 \\ \frac{U}{s} - \frac{u_{C_r0}}{s} + L_r \cdot i_{r0} + L_m \cdot i_{m0} \\ L_m \cdot i_{m0} + \frac{u_{C_o0}}{s} \\ \frac{u_{C_o0}}{s} \end{bmatrix} = \mathbf{A} \cdot \mathbf{x} \quad (8)$$

with

$$\mathbf{A} = \begin{bmatrix} -1 & 1 & 1 & 1 \\ \frac{1}{s \cdot C_r} + s \cdot L_r & s \cdot L_m & 0 & 0 \\ 0 & s \cdot L_m & -\frac{1}{s \cdot C_o} & 0 \\ 0 & 0 & -\frac{1}{s \cdot C_o} & R_o \end{bmatrix}, \quad (9)$$

the state vector

$$\mathbf{x} = \begin{bmatrix} I_r(s) \\ I_m(s) \\ I_c(s) \\ I_o(s) \end{bmatrix} \quad (10)$$

and the initial conditions i_{r0} , i_{m0} , u_{C_r0} and u_{C_o0} . Solving (8) results in

$$I_r(s) = \frac{(C_r R_o + C_r L_m s + C L_m R_o s^2) U}{D(s)} + \frac{(C_r L_r R_o s + C_r L_m L_r s^2) i_{r0}}{D(s)} + \frac{(C L_m L_r R_o s^3) i_{r0}}{D(s)} + \frac{(C_r L_m R_o s) i_{m0}}{D(s)} - \frac{(C_r R_o + C_r L_m s + C L_m R_o s^2) u_{C_r0}}{D(s)} - \frac{(C L_m R_o s^2) u_{C_o0}}{D(s)} \quad (11)$$

$$I_m(s) = \frac{(C_r R_o) U}{D(s)} + \frac{(C_r L_r R_o s) i_{r0}}{D(s)} + \frac{(L_m + C_o L_m R_o s + C_r L_m R_o s) i_{m0}}{D(s)} + \frac{(C_r L_m L_r s^2 + C L_m L_r R_o s^3) i_{m0}}{D(s)} - \frac{(C_r R_o) u_{C_r0}}{D(s)} - \frac{(C_o R_o + C L_r R_o s^2) u_{C_o0}}{D(s)} \quad (12)$$

$$I_c(s) = \frac{(C L_m R_o s^2) U}{D(s)} + \frac{(C L_m L_r R_o s^3) i_{r0}}{D(s)} - \frac{(C_o L_m R_o s + C L_m L_r R_o s^3) i_{m0}}{D(s)} - \frac{(C L_m R_o s^2) u_{C_r0}}{D(s)} - \frac{(C_o R_o + C_o L_m s + C L_m R_o s^2) u_{C_o0}}{D(s)} - \frac{(C L_r R_o s^2 + C L_m L_r s^3) u_{C_o0}}{D(s)} \quad (13)$$

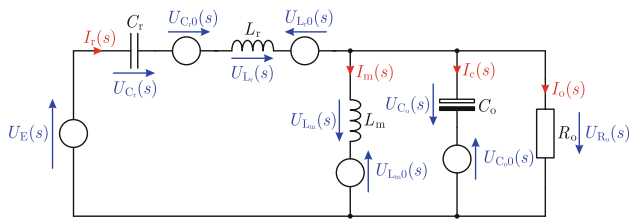


Fig. 6 Equivalent model for the interval $t \in \text{III}$

$$I_o(s) = \frac{(C_r L_m s) U}{D(s)} + \frac{(C_r L_m L_r s^2) i_{r0}}{D(s)} - \frac{(L_m + L_m C_r L_r s^2) i_{m0}}{D(s)} - \frac{(C_r L_m s) u_{C_r0}}{D(s)} + \frac{(L_m C_o s + C L_m L_r s^3) u_{C_o0}}{D(s)} \quad (14)$$

with $C = C_r C_o$ and with the denominator $D(s)$ given as

$$D(s) = (C_r L_r L_m C_o R_o) s^4 + (C_r L_r L_m) s^3 + (L_m C_o R_o + C_r L_m R_o + C_r L_r R_o) s^2 + (L_m) s + (R_o). \quad (15)$$

Please consider that these results take already into account that the equivalent systems are excited with a voltage step generated by the half bridge.

(15) can be rewritten to

$$D(s) = K \cdot (s - s_1)(s - s_2)(s - s_3)(s - s_4) \quad (16)$$

with $K = C_r L_r L_m C_o R_o$ and where s_i with $i \in \{1, 2, 3, 4\}$ are the zeros of the polynomial

$$P(s) = s^4 + \frac{C_r L_r L_m}{K} s^3 + \frac{L_m C_o R_o + C_r L_m R_o + C_r L_r R_o}{K} s^2 + \frac{L_m}{K} s + \frac{R_o}{K}, \quad (17)$$

whereas $D(s) = K \cdot P(s)$ is valid.

Calculating the zeros of the 4th order polynomial can be done by using methods of Ferrari and Cardano. Knowing the zeros allows a partial fractional decomposition of the state quantities in Laplace domain. The derivation of the corresponding time quantities is subsequently achieved with the Inverse Laplace Transformation. Other quantities describing the converter can simply be derived using algebraic manipulations.

Determining the time domain functions is straightforward using the partial fraction decomposition:

$$\frac{N(s)}{K \cdot P(s)} = \frac{A}{(s - s_1)} + \frac{B}{(s - s_2)} + \frac{C}{(s - s_3)} + \frac{D}{(s - s_4)}, \quad (18)$$

which is equivalent to

$$\frac{N(s)}{K} = A(s - s_2)(s - s_3)(s - s_4) + B(s - s_1)(s - s_3)(s - s_4) + C(s - s_1)(s - s_2)(s - s_4) + D(s - s_1)(s - s_2)(s - s_3). \quad (19)$$

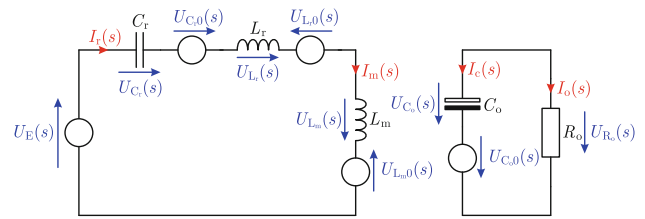


Fig. 7 Equivalent model for the interval $t \in \text{IV}$

The constants $A - D$ are then given by

$$A = \frac{N(s_1)}{K(s_1 - s_2)(s_1 - s_3)(s_1 - s_4)} \\ B = \frac{N(s_2)}{K(s_2 - s_1)(s_2 - s_3)(s_2 - s_4)} \\ C = \frac{N(s_3)}{K(s_3 - s_1)(s_3 - s_2)(s_3 - s_4)} \\ D = \frac{N(s_4)}{K(s_4 - s_1)(s_4 - s_2)(s_4 - s_3)}, \quad (20)$$

where $N(s)$ represents the numerator of the corresponding quantity. Thus, the constants A, B, C and D for all four state quantities can be calculated directly.

For the latter one can subsequently write

$$i_r = A_r \cdot e^{s_1 t} + B_r \cdot e^{s_2 t} + C_r \cdot e^{s_3 t} + D_r \cdot e^{s_4 t} \quad (21)$$

$$i_m = A_m \cdot e^{s_1 t} + B_m \cdot e^{s_2 t} + C_m \cdot e^{s_3 t} + D_m \cdot e^{s_4 t} \quad (22)$$

$$i_c = A_c \cdot e^{s_1 t} + B_c \cdot e^{s_2 t} + C_c \cdot e^{s_3 t} + D_c \cdot e^{s_4 t} \quad (23)$$

$$i_o = A_o \cdot e^{s_1 t} + B_o \cdot e^{s_2 t} + C_o \cdot e^{s_3 t} + D_o \cdot e^{s_4 t}. \quad (24)$$

Applying the well known correspondence $u_L = L \cdot \frac{di}{dt}$ while using (21) and (22) allows to calculate the inductor voltages

$$u_{L_r} = L_r (A_r \cdot s_1 e^{s_1 t} + B_r \cdot s_2 e^{s_2 t}) + L_r (C_r \cdot s_3 e^{s_3 t} + D_r \cdot s_4 e^{s_4 t}) \quad (25)$$

$$u_{L_m} = L_m (A_m \cdot s_1 e^{s_1 t} + B_m \cdot s_2 e^{s_2 t}) + L_m (C_m \cdot s_3 e^{s_3 t} + D_m \cdot s_4 e^{s_4 t}). \quad (26)$$

The voltage across the output capacitor of the simplified model is equal to the voltage across the magnetizing inductor for the considered case. Thus,

$$u_{C_o} = u_{L_m} \quad (27)$$

is valid.

Finally, the voltage across the resonant capacitor C_r can be determined by applying Kirchhoff's voltage law

$$u_{C_r} = U_B - u_{L_r} - u_{L_m}. \quad (28)$$

3.2 Derivation of the model for interval II and IV

For the separated model given in Fig. 5,

$$\frac{U_B}{s} = \frac{I_r(s)}{s C_r} + \frac{u_{C_r0}}{s} + I_r(s) s L_r - L_r i_{r0} + I_r(s) s L_m - L_m i_{r0} \quad (29)$$

is valid.

Please remind that for interval **IV**, U has to be replaced by $-U$ due to the inverted polarity (see also Figs. 5 and 7).

Solving for $I_r(s)$ leads to

$$I_r(s) = \frac{U_B C_r - C_r u_{C_r 0} + s i_{r0} (C_r L_r + C_r L_m)}{1 + s^2 (C_r L_r + C_r L_m)}. \quad (30)$$

Analog to the model valid for interval **I** and **III**, the denominator is given by

$$Q(s) = 1 + s^2 (C_r L_r + C_r L_m), \quad (31)$$

which can also be written as

$$Q(s) = M \cdot (s - s_5)(s - s_6) \quad (32)$$

with $M = C_r L_r + C_r L_m$, where s_i ($i \in \{5,6\}$) are the zeros of the polynomial

$$R(s) = s^2 + \frac{1}{M} \quad (33)$$

with $Q(s) = M \cdot R(s)$.

The two conjugate complex zeros are then given by

$$s_5, s_6 = \pm \frac{j}{\sqrt{C_r L_r + C_r L_m}}. \quad (34)$$

Following the same approach again,

$$\frac{T(s)}{M \cdot R(s)} = \frac{E}{(s - s_5)} + \frac{F}{(s - s_6)} \quad (35)$$

which is equivalent to

$$\frac{T(s)}{M} = E(s - s_6) + F(s - s_5) \quad (36)$$

can be determined and allows to find the constants with

$$\begin{aligned} E &= \frac{T(s_5)}{M(s_5 - s_6)}, \\ F &= \frac{T(s_6)}{M(s_6 - s_5)} \end{aligned} \quad (37)$$

where $T(s)$ is the numerator of the resonant current.

For the latter one finally finds

$$i_r = E \cdot e^{s_5 \cdot t} + F \cdot e^{s_6 \cdot t}. \quad (38)$$

In these two cases, the magnetizing current is equal to the resonant current

$$i_m = i_r = E \cdot e^{s_5 \cdot t} + F \cdot e^{s_6 \cdot t}. \quad (39)$$

The voltages across the inductors can again be calculated by derivation of (39) which results in

$$u_{L_r} = L_r (E \cdot s_5 e^{s_5 \cdot t} + F \cdot s_6 e^{s_6 \cdot t}) \quad (40)$$

$$u_{L_m} = L_m (E \cdot s_5 e^{s_5 \cdot t} + F \cdot s_6 e^{s_6 \cdot t}), \quad (41)$$

finally yielding to

$$u_{C_r} = U_B - u_{L_r} - u_{L_m}. \quad (42)$$

The second part of the decoupled model is given by

$$\frac{I_o(s)}{s C_o} + I_o(s) R_o - \frac{u_{C_o 0}}{s} = 0 \quad (43)$$

and the current $I_o(s)$ can be calculated to

$$I_o(s) = \frac{C_o \cdot u_{C_o 0}}{1 + s C_o R_o}. \quad (44)$$

Applying the Inverse Laplace Transformation on (44) directly leads to

$$i_o(t) = \frac{u_{C_o 0}}{R_o} \cdot e^{-\frac{t}{R_o C_o}}. \quad (45)$$

The capacitor current is equal to the output current with opposite sign in the considered time intervals, i.e.

$$i_c(t) = -i_o(t) = -\frac{u_{C_o 0}}{R_o} \cdot e^{-\frac{t}{R_o C_o}}, \quad (46)$$

finally leading to

$$u_{C_o} = u_{C_o 0} \cdot e^{-\frac{t}{R_o C_o}}. \quad (47)$$

3.3 Derivation of the Complete Solution

So, all quantities of the LLC resonant converter are known as a function of time, the component values, the bridge voltage U_B , as well as the initial conditions for each interval of the cycle.

For $t \in \mathbf{I}$, the model given in Fig. 4 is valid. The bridge voltage is $U_B = U$ and the currents through the inductors, as well as the voltages across the capacitors at the end of **I** can be calculated by inserting $t = t_x$. Those expressions, which are a function of the component values and the initial conditions at time instant $t = 0$, can subsequently be inserted for the initial conditions of the separated model valid during time interval **II**. Using the separated model given in Fig. 5 allows to calculate the initial conditions for the time interval **III** by inserting $t = \frac{T_s}{2} - t_x$.

For interval **III**, again the full model given in Fig. 6 is used. However, the bridge voltage $U_B = -U$ changes its sign. Accordingly, the polarity is inverted in Fig. 6 compared to Fig. 4. As the change of the voltage direction would discharge the output capacitor C_o in the used models, the initial condition for the voltage across the output capacitor C_o must be reversed as well. In order to compensate that, the sign of the affected quantities (output voltage u_{C_o} and output current i_o for the time intervals **III** and **IV**) has to be changed in the end. With this model, the initial conditions of interval **IV** can finally be determined.

At this point, the converter is fully described by the component values and the initial conditions at time

instant $t = 0$, assuming that U_B is given. Unfortunately this is not sufficient yet, as the initial conditions of the steady state operating point are not known in advance. Instead of doing several exhaustive iterations to derive the initial conditions, a novel approach is presented here.

As already mentioned, in steady state operation the voltage and current waveforms show half wave symmetry, i.e. $f(t) = -f(t - \frac{T_s}{2})$. The integral of each quantity over the full switching cycle must hence be zero! This relationship can be used advantageously to determine the initial conditions which provide the steady state immediately.

To find a unique solution for the four initial conditions, four equations are needed. Integrating the four currents and setting them to zero will not provide the solution, as the currents are linearly dependent on each other. To avoid that limitation, the output voltage can be included as a fifth part.

Due to analogy, the integral is only stated for the resonant current i_r . Hence

$$i_{r,int} = \int_0^{t_x} i_{r,I} d\tau + \int_0^{\frac{T_s}{2}-t_x} i_{r,II} d\tau + \int_0^{t_x} i_{r,III} d\tau + \int_0^{\frac{T_s}{2}-t_x} i_{r,IV} d\tau \quad (48)$$

is calculated.

The integral is applied in the same manner for i_m , i_c , i_o and u_{C_o} .

The lower integration limit is zero for each interval, as the related functions have been derived in a way so that the time variable is zero at the beginning of the corresponding interval.

For steady state condition,

$$\begin{aligned} i_{r,int} &\stackrel{!}{=} 0 \\ i_{m,int} &\stackrel{!}{=} 0 \\ i_{c,int} &\stackrel{!}{=} 0 \\ u_{C_o,int} &\stackrel{!}{=} R_o \cdot i_{o,int} \end{aligned} \quad (49)$$

must be valid accordingly.

Solving (49) finally leads to the initial conditions i_{r0} , i_{m0} , u_{C_r0} and u_{C_o0} , which provide steady state immediately. The expressions are not stated here as they are rather long. As a last step, the time t_x must be determined. The most obvious guess is $t_x = \frac{T_r}{2}$, where $T_r = \frac{1}{f_r}$. In a first step this is only a rough estimation, but it turned out to be a good starting point for an iterative process to find t_x . The process converges within a few iterations, providing a full description of the converter in steady state condition for a dedicated operating point. As one of the initial conditions is the voltage across the output capacitor, one directly receives the output voltage of the converter if the voltage-ripple is neglected.

To derive the correct value for t_x , the relationship

$$i_r(t_x) \stackrel{!}{=} i_m(t_x) \quad (50)$$

can be used, which is equivalent to

$$f(t_x) = i_r(t_x) - i_m(t_x) \stackrel{!}{=} 0, \quad (51)$$

as this must be valid at $t = t_x$.

The analytical expressions of i_r and i_m are known and Newton's Approximation Method can be applied to calculate t_x .

Hence

$$t_{x,n+1} = t_{x,n} - \frac{f(t_{x,n})}{f'(t_{x,n})} \quad (52)$$

with the iteration variable $n \in \mathbb{N}_0$, using $t_{x,0} = \frac{T_r}{2}$ as a start value just as aforementioned has to be implemented, finally converging to the optimal value for t_x according to

$$t_{x,opt} = t_{x,n_{max}} \quad (53)$$

with

$$|t_{x,n_{max}+1} - t_{x,n_{max}}| \leq \epsilon. \quad (54)$$

Simulation results in the following section verify, that this approach is describing the current and voltage conditions with high accuracy for different operating points. The models are used in a predefined order, assuming that the resonant current differs from the magnetizing current for $0 < t < t_x$ and $\frac{T_s}{2} < t < \frac{T_s}{2} + t_x$ and that the latter are the same for $t_x \leq t \leq \frac{T_s}{2}$ and $\frac{T_s}{2} + t_x \leq t \leq T_s$ as it is depicted in Fig. 3.

3.4 Model Summary

The calculation steps of the proposed analytical model are summarized in Fig. 8. Before applying the model, the full parameter set $\mathcal{S} = \{U_B, f_s, C_r, L_r, L_m, \frac{N_1}{N_2}, C_{o,s}, R_{o,s}\}$

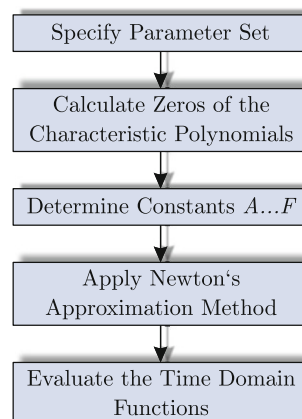


Fig. 8 Calculation of the proposed analytical model

must be defined first. Subsequently, the zeros of the polynomials $P(s)$ and $R(s)$ given in (17) and (33) can be determined, leading to the parameters $A_{\mathcal{U}}, B_{\mathcal{U}}, C_{\mathcal{U}}, D_{\mathcal{U}}, E, F$ with $\mathcal{U} = \{r, m, c, o\}$, as stated in (20) and (37) respectively.

With these parameters, the complete solution is known as a function of the initial conditions i_{r0}, i_{m0}, u_{C_r0} and u_{C_o0} , as well as of t_x . The initial conditions as a function of t_x leading to steady state can be obtained by solving (49). The time instant t_x can be determined easily by applying Newtons Approximation Method (52)–(54).

Having $t_{x,opt}$, all interval boundaries as well as the initial conditions are set. The voltage and current waveforms can be calculated by evaluating the time functions of the corresponding intervals.

4 Simulation Results

To verify the proposed model, the operating points listed in Table 1 are used. Calculated results using the proposed model are compared to time domain simulation results, using PLECS simulation software as shown in Table 2. At first the comparison is made regarding the RMS value of the resonant current, as it is decisive for determining conduction losses. Secondly, the average value of the output voltage is compared to determine the accuracy of the proposed model. Finally, also the obtained RMS values of the resonant current when applying the FHA method are listed in Table 2 for comparative purposes.

Within the first three operating points, the switching frequency is varied. Due to parameter selection, the characteristic resonance frequency is set to $f_r = 5.033$ kHz. Thus, the chosen switching frequencies provide results for operation far below resonance (# 1), nearly RO (#2), as well as for an arbitrary operating point in between (#3).

For the latter, the time domain voltages as well as the time domain currents calculated with the proposed model are given in Figs. 9 and 10 respectively. The results obtained from the PLECS simulation are not depicted as they are basically the same (see Table 2). Both figures show the characteristic and expected waveforms for the intended operating mode. Moreover, the output voltage is compared to the result taken from time simulations using PLECS simulation

Table 1 Operating points used to verify the novel analytical model

#	R_o	f_s	ϵ	n_{max}
1	10 Ω	3 kHz	10^{-6}	1
2	10 Ω	5 kHz	10^{-6}	1
3	10 Ω	4 kHz	10^{-6}	2
4	5 Ω	4 kHz	10^{-6}	2
5 ¹	100 Ω	15 kHz	10^{-6}	2
6 ²	10 Ω	30 kHz	10^{-6}	1

Parameter values: $U = 416$ V, $C_r = 10$ μ F, $L_r = 0.1$ mH, $L_m = 1$ mH, $C_o = 3$ mF;
¹ $C_r = 1$ μ F;
² $C_r = 1$ μ F, $L_r = 10$ μ H, $L_m = 0.1$ mH

software, as shown in Fig. 11. It appears that the results fit almost perfectly. The same is valid for the other operating points listed in Table 1. The relative deviations can be withdrawn from Table 2 and validate the proposed models ability to determine the output voltage which has to be expected.

For operating point # 2, a comparison of the resonant currents is given in Fig. 12. As the switching frequency is very close to the resonance frequency in this case, it almost looks like RO operation mode. However, the relative deviation is negligible as it is also valid for other operating points given in Table 1. Thus, the models applicability over the whole frequency range in OBR operation mode is verified.

For operating point #4, the frequency is kept unchanged compared to operating point # 3, but the load is increased. The resonant current i_r is now higher, while the output voltage is nearly unchanged, which is a characteristic behavior of the considered converter. Also the precision of the model is not afflicted by the load change.

For operating point # 5, the switching frequency f_s has been increased to 15 kHz. While the relative deviation for the RMS value of the resonant current ($\Delta i_{r,rel}$) is below approximately 0.2% for other operating points addressed in this paper, it is about 1.5% here. This seemingly significant error increase, however, is just due to the comparably small resonant current. When comparing the absolute deviation, which accumulates to $\Delta i_{r,abs} = 100$ mA here, the discrepancy is within the same range as for other operating points considered (e.g. # 2).

Table 2 Comparison of PLECS simulations with the proposed model and FHA

PLECS Simulation		Proposed Analytical Model				FHA		
#	$i_{r,RMS}$	$u_{C_o,AVG}$	$i_{r,RMS}$	$\Delta i_{r,rel}$	$u_{C_o,AVG}$	$\Delta u_{C_o,rel}$	$i_{r,RMS}$	$\Delta i_{r,rel}$
1	75.57 A	503.03 V	75.59 A	0.026%	503.01 V	-0.004%	54.62 A	-27.72%
2	48.67 A	416.68 V	48.77 A	0.205%	416.66 V	-0.005%	47.77 A	-1.86%
3	56.54 A	444.81 V	56.56 A	0.035%	444.82 V	0.002%	50.63 A	-10.45%
4	113.77 A	444.28 V	113.81 A	0.035%	444.28 V	0.001%	92.79 A	-18.44%
5	6.74 A	422.49 V	6.64 A	-1.484%	422.46 V	-0.007%	6.17 A	-8.50%
6	75.53 A	503.08 V	75.63 A	0.132%	503.03 V	-0.010%	54.68 A	-27.60%

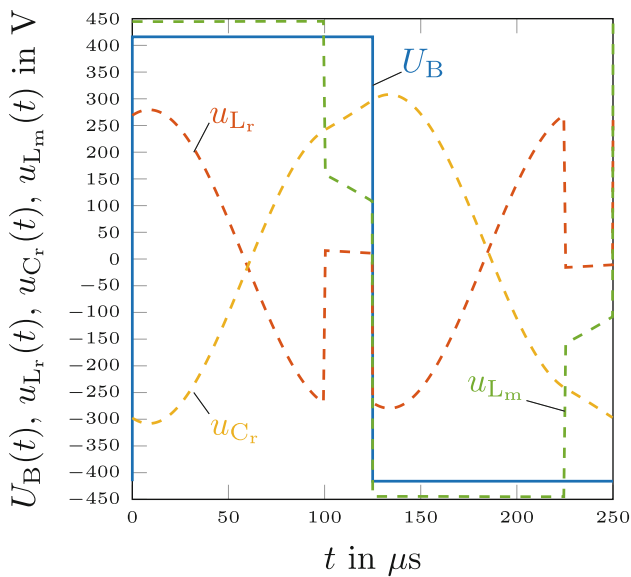


Fig. 9 Bridge voltage (U_B) and calculated voltage across the resonant inductor (u_{L_r}), resonant capacitor (u_{C_r}), magnetizing inductor (u_{L_m}) for operating point # 3

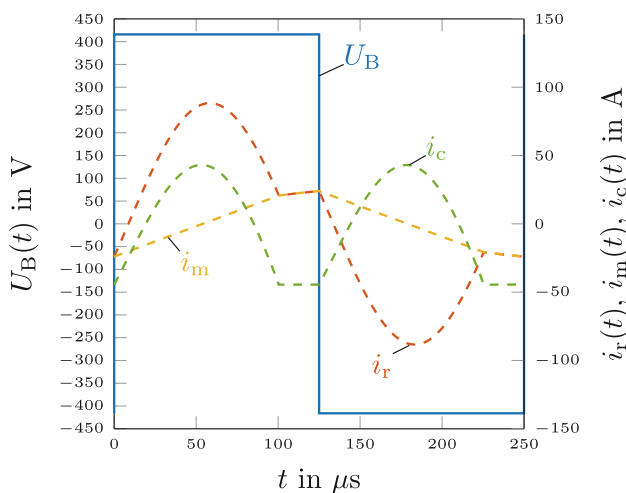


Fig. 10 Bridge voltage (U_B) and calculated resonant current (i_r), magnetizing current (i_m), and current through the output capacitor (i_c) for operating point # 3

For operating point # 6, the switching frequency finally has been increased even further to about $f_s = 30\text{kHz}$, allowing to verify that the model performs properly even at higher switching frequencies.

Having a closer look into Table 1, it appears that the number of required iterations n_{\max} is very small. For some operating points it is even one, which allows it to interpret those solutions as exclusively analytic ones without a single required iteration.

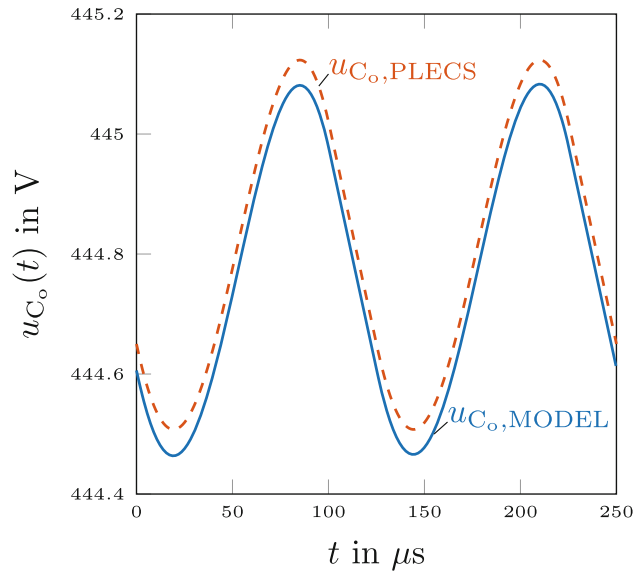


Fig. 11 Output voltage comparison between the model calculation ($u_{C_o,MODEL}$) and the PLECS simulation ($u_{C_o,PLECS}$) for operating point # 3

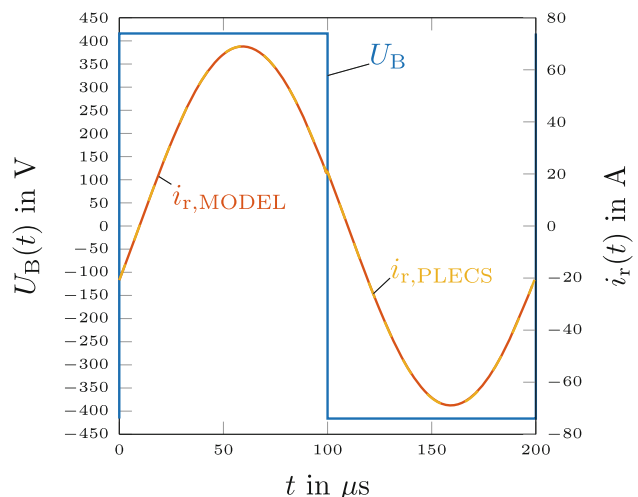


Fig. 12 Bridge voltage (U_B) and resonant current comparison between model ($i_{r,MODEL}$) and PLECS simulation ($i_{r,PLECS}$) for operating point # 2

5 Conclusion

In this paper, a strategy for describing the behavior of the ideal LLC resonant converter in OBR operating mode has been introduced. Promising simulation results show, that the converter quantities are depicted quite accurate, which in turn directly allows to use this strategy for converter cell design. This is possible, as the suggested strategy unlike the aforementioned FHA, is able to compute the output voltage sufficiently accurate. Also, it has been shown that a very small number of iteration steps is needed to obtain these solutions. Hence the time consumption can be kept at a low level, which is desirable if huge parameter

sets have to be considered during optimization in order to find the optimum. Please keep in mind that the converter is still considered to be ideal and the operating range is restricted here. However, the proposed method can be easily augmented to RO operating mode, as well as OAR operating mode if needed.

Funding Open access funding provided by Graz University of Technology.

Open Access This article is licensed under a Creative Commons Attribution 4.0 International License, which permits use, sharing, adaptation, distribution and reproduction in any medium or format, as long as you give appropriate credit to the original author(s) and the source, provide a link to the Creative Commons licence, and indicate if changes were made. The images or other third party material in this article are included in the article's Creative Commons licence, unless indicated otherwise in a credit line to the material. If material is not included in the article's Creative Commons licence and your intended use is not permitted by statutory regulation or exceeds the permitted use, you will need to obtain permission directly from the copyright holder. To view a copy of this licence, visit <http://creativecommons.org/licenses/by/4.0/>.

References

- Bhat A (1994) Analysis and design of lcl-type series resonant converter. *IEEE Trans Ind Electron* 41(1):118–124. <https://doi.org/10.1109/41.281617>
- Channegowda J, Pathipati VK, Williamson SS (2015) Comprehensive review and comparison of dc fast charging converter topologies: Improving electric vehicle plug-to-wheels efficiency. In: 2015 IEEE 24th International Symposium on Industrial Electronics (ISIE), pp 263–268 <https://doi.org/10.1109/ISIE.2015.7281479>
- Chen R, Yu S (2018) A high-efficiency high-power-density 1mhz llc converter with gan devices and integrated transformer. In: 2018 IEEE Applied Power Electronics Conference and Exposition (APEC), pp 791–796 <https://doi.org/10.1109/APEC.2018.8341102>
- Choi H (2007) Analysis and design of llc resonant converter with integrated transformer. In: APEC 07 - Twenty-Second Annual IEEE Applied Power Electronics Conference and Exposition, pp 1630–1635 <https://doi.org/10.1109/APEX.2007.357736>
- De Simone S, Adragna C, Spini C, Gattavari G (2006) Design-oriented steady-state analysis of llc resonant converters based on fha. In: International Symposium on Power Electronics, Electrical Drives, Automation and Motion, 2006. SPEEDAM 2006, pp 200–207 <https://doi.org/10.1109/SPEEDAM.2006.1649771>
- Fang X, Hu H, Chen L, Amirahmadi A, Shen J, Batarseh I (2012) Operation analysis and numerical approximation for the llc dc-dc converter. In: 2012 Twenty-Seventh Annual IEEE Applied Power Electronics Conference and Exposition (APEC), pp 870–876 <https://doi.org/10.1109/APEC.2012.6165921>
- Fang X, Hu H, Shen ZJ, Batarseh I (2012) Operation mode analysis and peak gain approximation of the LLC resonant converter. *IEEE Trans Power Electron* 27(4):1985–1995. <https://doi.org/10.1109/TPEL.2011.2168545>
- Fei C, Lee FC, Li Q (2017) High-efficiency high-power-density llc converter with an integrated planar matrix transformer for high-output current applications. *IEEE Trans Ind Electron* 64(11):9072–9082. <https://doi.org/10.1109/TIE.2017.2674599>
- Jiao J, Guo X, Wang C, You X (2022) Time-domain analysis and optimal design of llc-dc transformers (llc-dcxs) considering discontinuous conduction modes. In: IEEE Transactions on Transportation Electrification, pp 1–1 <https://doi.org/10.1109/TTE.2022.3205954>
- Lazar J, Martinelli R (2001) Steady-state analysis of the llc series resonant converter. In: APEC 2001. Sixteenth Annual IEEE Applied Power Electronics Conference and Exposition (Cat. No. 01CH37181), vol 2, pp 728–735 <https://doi.org/10.1109/APEC.2001.912451>
- Liu J, Zhang J, Zheng TQ, Yang J (2017) A modified gain model and the corresponding design method for an llc resonant converter. *IEEE Trans Power Electron* 32(9):6716–6727. <https://doi.org/10.1109/TPEL.2016.2623418>
- Mortazavizadeh SA, Palazzo S, Amendola A, De Santis E, Di Ruzza D, Panariello G, Sanseverino A, Velardi F, Busatto G (2021) High frequency, high efficiency, and high power density gan-based llc resonant converter: State-of-the-art and perspectives. *Appl Sci* 11(23):11350. <https://doi.org/10.3390/app112311350>
- Oeder C, Duerbaum T (2013) Zvs investigation of llc converters based on fha assumptions. In: 2013 Twenty-Eighth Annual IEEE Applied Power Electronics Conference and Exposition (APEC), pp 2643–2648 <https://doi.org/10.1109/APEC.2013.6520669>
- Safayatullah M, Elrais MT, Ghosh S, Rezaii R, Batarseh I (2022) A comprehensive review of power converter topologies and control methods for electric vehicle fast charging applications. *IEEE Access* 10:40753–40793. <https://doi.org/10.1109/ACCESS.2022.3166935>
- Schröder D, Marquardt R (2019) Leistungselektronische Schaltungen Funktion, Auslegung und Anwendung: Funktion, Auslegung und Anwendung <https://doi.org/10.1007/978-3-662-55325-1>
- Shafiei N, Sabet MA, Ordóñez M (2017) Time domain analysis of llc resonant converters in the boost mode for battery charger applications. In: 2017 IEEE Energy Conversion Congress and Exposition (ECCE), pp 4157–4162 <https://doi.org/10.1109/ECCE.2017.8096721>
- Steigerwald R (1988) A comparison of half-bridge resonant converter topologies. *IEEE Trans Power Electron* 3(2):174–182. <https://doi.org/10.1109/63.4347>
- Tu H, Feng H, Srdic S, Lukic S (2019) Extreme fast charging of electric vehicles: A technology overview. *IEEE Trans Transp Electrific* 5(4):861–878. <https://doi.org/10.1109/TTE.2019.2958709>

Publisher's Note Springer Nature remains neutral with regard to jurisdictional claims in published maps and institutional affiliations.



Daniel Neuner, received the BSc and the MSc degree in electrical engineering from Graz University of Technology (TU Graz), Graz, Austria in 2019 and 2022, respectively. In February 2022, he joined the power electronics research group at the Electric Drives and Machines Institute (EAM), TU Graz, as a university assistant and PhD student. His research interests include resonant converter design and control, especially for application in high power chargers.



Michael Hartmann, received the B.Sc. and M.Sc. (Hons.) degrees in electrical engineering from the Vienna University of Technology, Vienna, Austria, in 2005 and 2006, respectively. In 2011, he received the Ph.D. degree from the Swiss Federal Institute of Technology (ETH), Zurich, Switzerland. In 2011 he joined Schneider Electric Power Drives in Vienna where he was involved in the research on high efficiency and compact three-phase power converter systems for low- and medium-voltage power drives. In 2012 he received the IEEE PELS Transaction Prize Paper Award. Since 2021 he is appointed as Full Professor for power electronics at the Electric Drives and Machines Institute of Graz University of Technology (TU-Graz), Graz, Austria.